Propagating Annular Modes: Empirical Orthogonal Functions, Principal Oscillation Patterns, and Time Scales

ADITI SHESHADRI

Department of Applied Physics and Applied Mathematics, Columbia University, New York, New York

R. ALAN PLUMB

Department of Earth, Atmospheric, and Planetary Sciences, Massachusetts Institute of Technology, Cambridge, Massachusetts

ABSTRACT

The two leading empirical orthogonal functions (EOFs) of zonal-mean zonal wind describe north–south fluctuations, and intensification and narrowing, respectively, of the midlatitude jet. Under certain circumstances, these two leading EOFs cannot be regarded as independent but are in fact manifestations of a single, coupled, underlying mode of the dynamical system describing the evolution in time of zonal wind anomalies. The true modes are revealed by the principal oscillation patterns (POPs). The leading mode and its associated eigenvalue are complex, its structure involves at least two EOFs, and it describes poleward (or equatorward) propagation of zonal-mean zonal wind anomalies. In this propagating regime, the principal component (PC) time series associated with the two leading EOFs decay nonexponentially, and the response of the system to external forcing in a given EOF does not depend solely on the PC decorrelation time nor on the projection of the forcing onto that EOF. These considerations are illustrated using results from an idealized dynamical core model. Results from Southern Hemisphere ERA-Interim data are partly consistent with the behavior of the model's propagating regime. Among other things, these results imply that the time scale that determines the sensitivity of a model to external forcing might be different from the decorrelation time of the leading PC and involves both the rate of decay of the dynamical mode and the period associated with propagation.

1. Introduction

The leading modes of variability of the extratropical circulation are usually referred to as the "annular modes" (e.g., Thompson and Wallace 2000; Thompson et al. 2000) and are derived from empirical orthogonal function (EOF) analysis of meteorological fields such as geopotential height or zonal-mean zonal wind (Kidson 1988; Lorenz and Hartmann 2001, 2003). The leading EOF of zonal-mean zonal wind takes the form of a dipolar structure centered on the time-mean jet and describes north–south fluctuations in time of the jet. The second EOF peaks at the maximum of the time-mean jet, and, independently, it describes intensification and narrowing ("pulsing") of the midlatitude jet. However, the leading EOFs of zonal wind are not necessarily independent of each other and, together, the two leading EOFs may describe the poleward propagation of zonal wind anomalies. Such propagation has been noted in models (e.g., James and Dodd 1996; Lee et al. 2007) and in both Northern and Southern Hemisphere observations (Feldstein 1998) and is illustrated for Southern Hemisphere wind anomalies by the examples shown in Fig. 1. Periods of both propagation and nonpropagation are evident, in all seasons; propagating anomalies typically appear in low latitudes and migrate generally poleward over the course of 2–3 months, although there are some instances of equatorward propagation. In terms of the leading EOFs, propagation is manifested through nonzero lag correlations between the two corresponding principal components (Lorenz and Hartmann 2001; Son and Lee 2006; Watterson 2007; Sparrow et al. 2009). For the examples shown in Fig. 1, reconstructions based on the projections onto the two leading EOFs of zonal-mean zonal wind are shown in Fig. 2; most of the midlatitude variability, including propagation when it occurs, is reproduced by these two

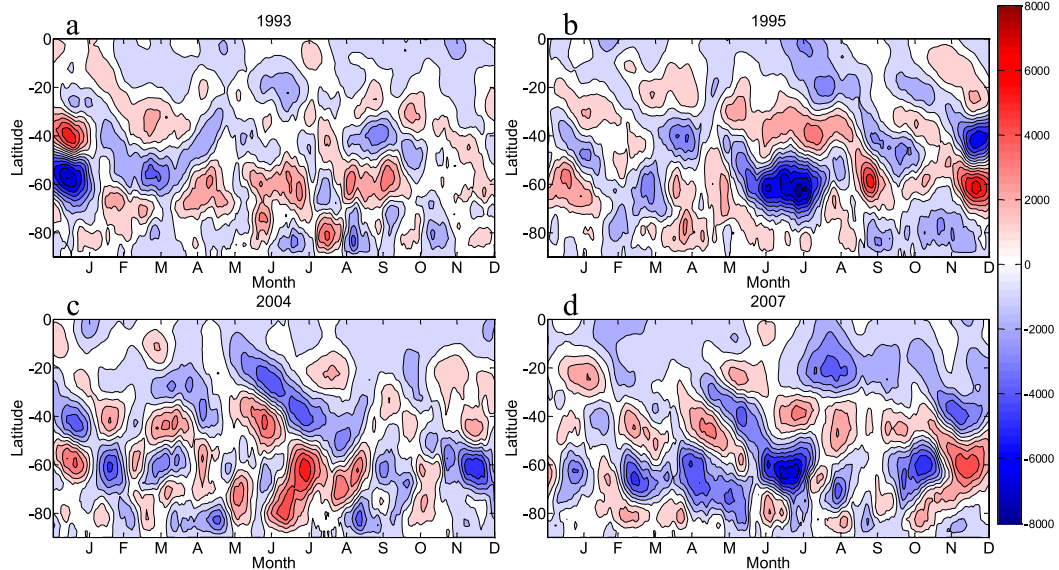*Corresponding author e-mail*: Aditi Sheshadri, as4915@columbia.edu

FIG. 1. Zonal-mean zonal wind anomalies from ERA-Interim data (daily anomalies from a seasonal climatology smoothed using a 21-day centered moving average) integrated across the depth of the troposphere (925–100 hPa) for the Southern Hemisphere in (a) 1993, (b) 1995, (c) 2004, and (d) 2007. The contour interval is 1000 hPa m s^{-1}.

components, but much of the variability in low and high latitudes is not. Among other things, Son and Lee (2006) explored the circumstances under which the leading modes of variability of a simplified dynamical core model take the form of nonpropagating or propagating anomalies. When the climatology exhibits a single jet, they found nonpropagating behavior, for which the variance is dominated by a single EOF; with a double jet, zonal wind anomalies propagate poleward, the variance associated with the second EOF exceeding about one-half of that associated with the first.

In this paper we explore the characteristics of variability in the propagating regime. We shall argue that under such circumstances the leading, coupled, EOFs form a single underlying mode of the system, such that
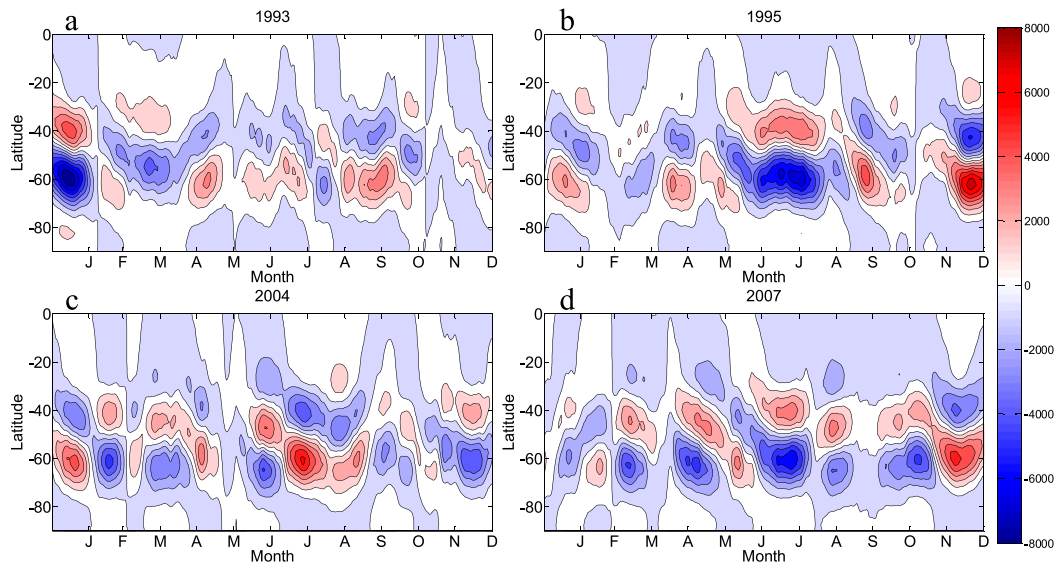

FIG. 2. Zonal-mean zonal wind anomalies from ERA-Interim data in Fig. 1, reconstructed from projections onto the two leading EOFs of zonal-mean zonal wind and smoothed using a 21-day centered moving average. The contour interval is 1000 hPa m s^{-1}.

individual EOFs cannot be properly regarded as "modes." One consequence of this is that the autocorrelations of the leading principal components (PCs) corresponding to the individual EOFs do not decay exponentially but show some oscillatory characteristics. This behavior, in turn, cautions against using simple paradigms based on stochastically forced, single component, systems as a basis for estimating eddy feedback strength (e.g., Lorenz and Hartmann 2001, 2003; Watterson 2007; Chen and Plumb 2009) or for estimating the sensitivity of the system to climate perturbations (Gerber et al. 2008; Ring and Plumb 2008).

Such questions are addressed here by application of theory to results from a dry, dynamical core, global model run in a simplified solsticial configuration. The model setup and climatology are described briefly in section 2. In section 3 it is shown that the leading modes of variability of the zonal jets are nonpropagating in the "summer" hemisphere and propagating in the "winter" hemisphere. These two differing types of anomaly are then used to illustrate the theoretical development of the paper. The dynamical modes of the zonal-mean flow system are identified in section 4 through calculation of the principal oscillation patterns (POPs; von Storch et al. 1988; Penland 1989). In the nonpropagating case, the leading POP is essentially identical to the dominant EOF, with a real eigenvalue corresponding to the de-correlation rate of the dominant PC, as found by Ring and Plumb (2008). In the propagating regime, on the other hand, the leading POP and its corresponding eigenvalue are complex; the structure of this single, propagating, mode involves at least two EOFs. The theoretical implications are explored in section 5, in which the characteristics of PC auto- and cross correlations in a stochastically forced system are described, with some remarks made about the implications for the response of the jets to climate perturbations. Finally, in section 6 we discuss the characteristics of the observed Southern Hemisphere zonal flow in the light of these results.

2. Model details

The dynamical core model is similar to that of Polvani and Kushner (2002), with some modifications as described below. The model is dry and hydrostatic, solving the global primitive equations with T42 resolution in the horizontal and 40 sigma levels in the vertical. There is no surface topography. Radiation and convection schemes are replaced by relaxation to a zonally symmetric equilibrium temperature profile identical to Held and Suarez (1994) in the troposphere. In the stratosphere (above 200 hPa), the equilibrium

temperature profile is a perpetual-solstice version of the equilibrium temperature specifications used in Sheshadri et al. (2015), with winter conditions in the Southern Hemisphere. As will be seen below, these choices result in a model configuration with reasonable annular mode time scales in the Southern Hemisphere. The model was run for 13 000 days, and the last 10 000 days are used in the analysis.

The time-averaged zonal-mean zonal wind is shown in Fig. 3. There is a single deep tropospheric jet near 35°N in the Northern Hemisphere; in the Southern Hemisphere, an upper-tropospheric subtropical jet near 30°S, a deeper midlatitude jet near 45°S, and a polar night jet near 60°S extending through the stratosphere. Note the hemispheric asymmetry of the zonal-mean zonal winds even in the troposphere, where the equilibrium temperature is symmetric about the equator. For simplicity, we shall refer to the Northern and Southern Hemispheres as summer and winter, respectively, even though there is no such contrast in the tropospheric equilibrium temperature.

3. EOFs of zonal-mean wind variability

The characteristics of flow variability in the atmosphere are commonly described using principal component analysis, in which the space–time fluctuations of the flow are separated via singular value decomposition

$$\mathbf{X} = \mathbf{U}\mathbf{\Sigma}\mathbf{V}^{\mathrm{T}} \qquad (1)$$

into spatial structures described by EOFs (the columns of $\mathbf{U}$) and temporal structures described by the corresponding PCs (the columns of $\mathbf{V}$ contain the normalized PCs), with $\mathbf{\Sigma}$ being the diagonal matrix[1] containing the corresponding singular values σ. While the EOFs compactly and efficiently describe the fluctuations (the contribution of each to the total variance being proportional to σ^2) and are frequently referred to as modes (such as the annular modes that are our focus here), they are not necessarily modes in the usual physical sense of being eigenmodes of the underlying dynamical system. Rather, just as the variability they describe, the EOFs and corresponding PCs depend on how the system is forced to produce the variability, and not just on the properties of the system modes themselves. Moreover, they are by design orthogonal ($\mathbf{U}^{\mathrm{T}}\mathbf{U} = \mathbf{I} = \mathbf{V}^{\mathrm{T}}\mathbf{V}$) whereas in general the system modes are not.

We consider here the EOFs of the zonal-mean zonal wind fluctuations below 100 hPa and poleward of 20°

---

[1] Here, and throughout this paper, we adopt the notation that diagonal matrices are represented by uppercase Greek characters.
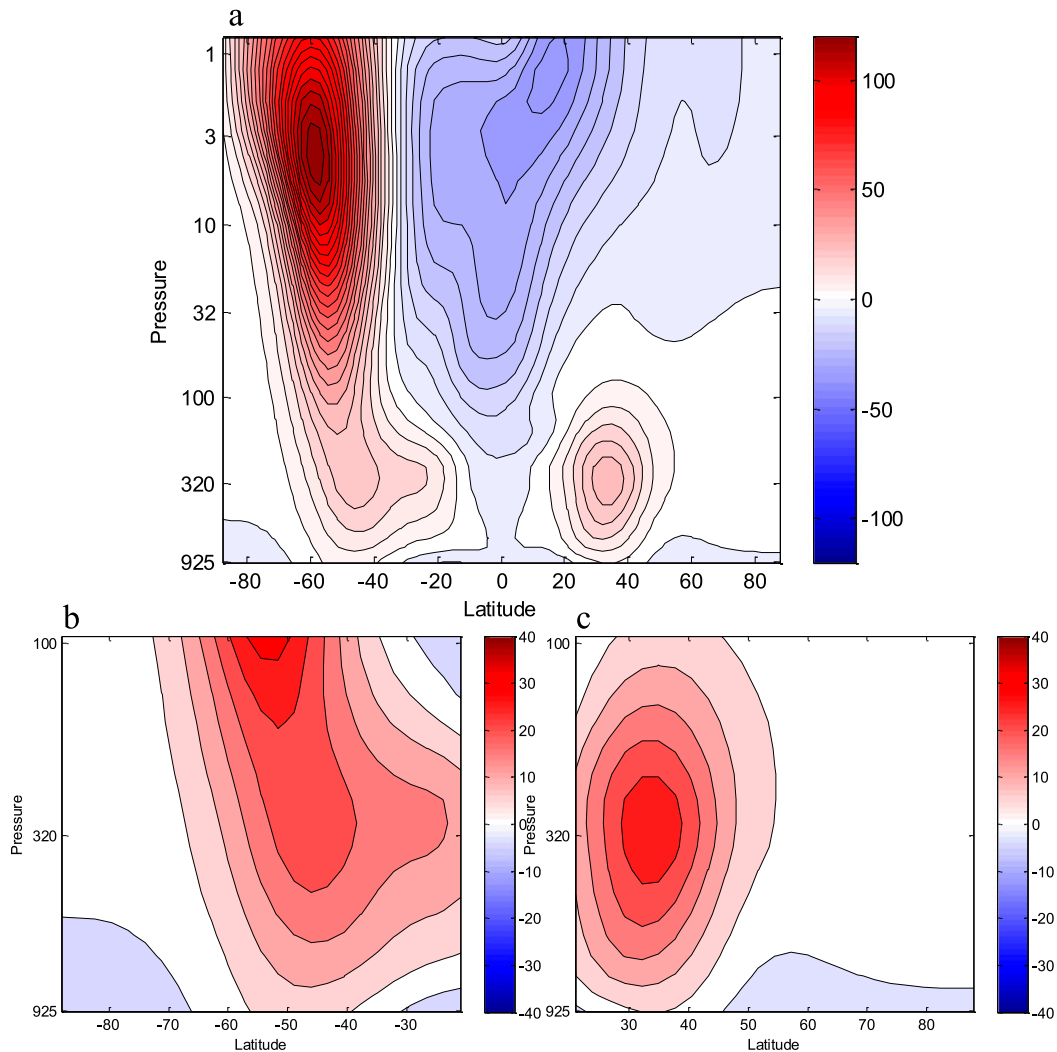
FIG. 3. Time-averaged zonal-mean zonal wind $(m\,s^{-1})$ (a) in both hemispheres in the model, (b) using tropospheric data for the Southern Hemisphere poleward of 20°S, and (c) using tropospheric data for the Northern Hemisphere poleward of 20°N. The control interval is $5\,m\,s^{-1}$.

latitude. To weight each data point appropriately, the variable used to perform (1) is $\sqrt{\delta p\,\cos\phi}(\overline{u} - [\overline{u}])$, where δp is the pressure thickness of the model level, ϕ is latitude, and the square brackets represent the time average of daily data and the overbar the zonal average; the EOFs of zonal wind are then $U_n(\phi, p)(\delta p\,\cos\phi)^{-1/2}$. The first two EOFs in the winter hemisphere are shown in Fig. 4. The EOF structures are similar to those seen in Southern Hemisphere data (e.g., Lorenz and Hartmann 2001; Fig. 11, below) and in models of this type (Son and Lee 2006; Sparrow et al. 2009; A. Sheshadri and R. A. Plumb 2016, unpublished manuscript): EOF1 is primarily a dipole straddling the midlatitude jet; EOF2 is also predominantly dipolar, but with its central extremum coincident with the latitude of the jet. Each makes a substantial contribution, 40% and 29%, respectively, to

the total zonal-mean wind variance. Taken separately, as has been noted many times previously, EOF1 describes latitudinal fluctuations of the midlatitude jet location, whereas EOF2 describes alternate strengthening and narrowing, and weakening and broadening, of the jet. The PC autocorrelations are shown in Fig. 4c. In a stable system subjected to white-noise forcing, for a single mode in isolation, the autocorrelation decays exponentially with lag (Hasselmann 1976); fitting an exponential to each curve over a lag of 30 days separately yields decorrelation times of 19 and 13 days. Lorenz and Hartmann (2001), finding similar results from their analysis of Southern Hemisphere data, ascribed this difference to eddy feedback acting on EOF1 but not EOF2, but we shall arrive in what follows at a different explanation. In fact, the dependence on lag of
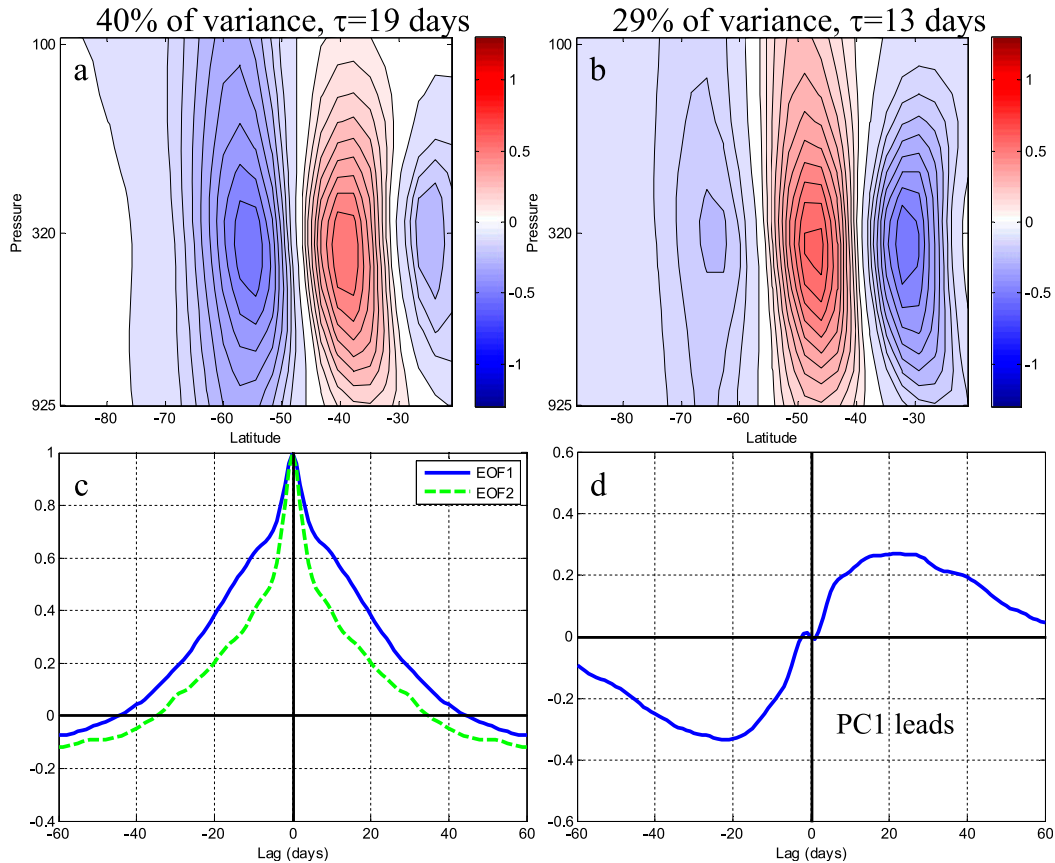
FIG. 4. The (a) first and (b) second EOFs of zonal-mean wind in the winter hemisphere of the model (determined from data poleward of 20°S). These two EOFs explain 40% and 29% of the zonal wind variance, respectively. (c) The autocorrelation function of these modes and (d) their cross correlation.

the autocorrelations differs from an exponential decay in two ways. The features evident at lags less than about 10 days can be ascribed to the finite time scale of the eddy forcing, which is not white but has memory over times characteristic of baroclinic eddy life cycles (Watterson 2002; Chen and Plumb 2009). The change of sign of both autocorrelations near 40-day lag requires a different explanation, a hint of which is provided by Fig. 4d, which shows the lag correlation between PCs 1 and 2. Despite the orthogonality of the PCs (which requires only that the cross correlation vanishes at zero lag) there is a significant lag correlation peaking at around ±20 days. This characteristic, noted by Lorenz and Hartmann (2001) and discussed in depth by Son and Lee (2006) and Sparrow et al. (2009), is such that positive PC1 → positive PC2 → negative PC1, thus implying a change of sign of PC1 and PC2 over 40 days. The sense of the cross correlation, given the relative structure of the EOFs, describes the poleward propagation of zonal wind anomalies, consistent with what has been reported in models and observations, and which is also evident here, as shown in Figs. 5a and 5c.

This behavior should be contrasted with that of the fluctuations of zonal wind in the summer hemisphere of the model. Figure 6 shows the leading EOFs for that case. The structures of the EOFs show characteristics similar to those in the winter hemisphere, with EOF1 dominated by a dipole straddling the climatological jet at 35°; EOF2 is also dipolar but with one of its extrema nearly coincident with the jet. In this case, however, EOF1 is dominant: it accounts for 62% of the variance, compared to 12% for EOF2, and the decorrelation times of the corresponding PCs are very different (68 vs 20 days). Further, the cross correlation between the two EOFs is very weak, implying that they act independently. As Fig. 5b illustrates, one consequence of this is the absence of propagation of the wind anomalies; Fig. 5d shows that EOF1 is sufficient to capture the evolution of zonal-mean zonal wind anomalies. Also evident in Fig. 5b is the remarkable longevity of zonal wind anomalies, consistent with the long decorrelation time of EOF1. Such unrealistically long decorrelation times are often found in this kind of model (Gerber et al. 2008) and,
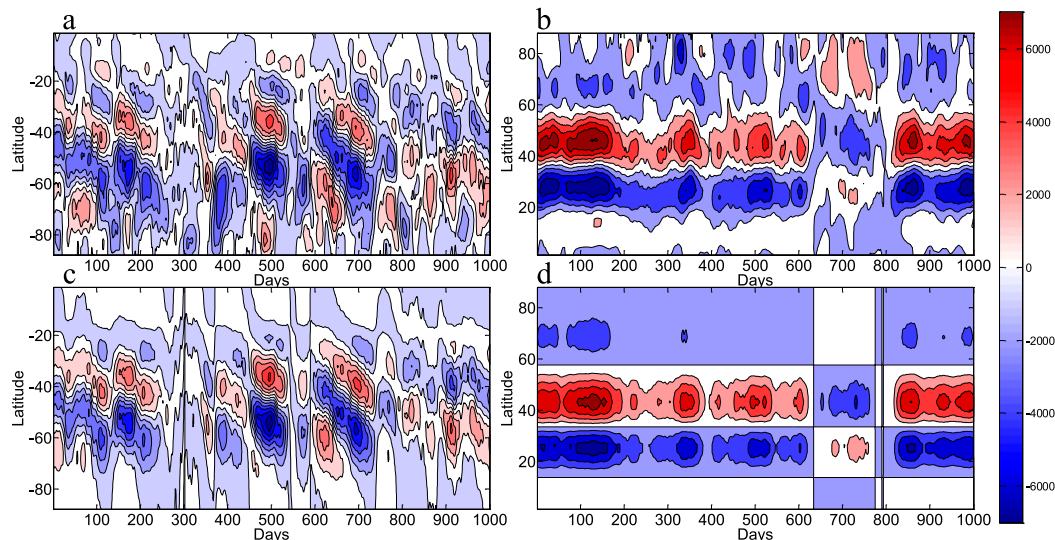
FIG. 5. Plots of 1000 days of zonal-mean zonal wind anomalies (daily values smoothed using a 21-day centered moving average) integrated across the depth of the troposphere (925–100 hPa) for the (a) Southern, "winter," and (b) Northern, "summer," Hemispheres, and the extent to which this is captured by (c) a combination of EOFs 1 and 2 for the winter hemisphere and (d) EOF1 for the summer hemisphere. The contour interval is 1000 hPa m s^{-1}.

indeed, Chan and Plumb (2009) found them to be especially long when the climatological subtropical and midlatitude jets are merged, as is the case here (Fig. 3).

Before leaving this section, it should be emphasized that the distinction between propagating and nonpropagating anomalies is not necessarily one associated with the difference between winter and summer, even though this is the case here. For example, in a troposphere-only model, Ring and Plumb (2007, 2008) found a single dominant mode in each hemisphere. Rather, the two cases illustrated here as winter and summer should be seen as illustrative of two distinct patterns of behavior that can be found under different conditions. Note also that the separation into the propagating and nonpropagating regimes is consistent with the results of Son and Lee (2006), who found that propagation occurs whenever the subtropical and midlatitude jets are separated, and when the variance described by EOF2 exceeds about one-half of that described by EOF1.

4. Principal oscillation patterns

a. Theory

We consider a forced, linear, dynamical system of the form

$$\frac{\partial \mathbf{u}}{\partial t} + \mathbf{A}\mathbf{u} = \mathbf{f}. \tag{2}$$

An equation of this form has been used to describe fluctuations of zonal-mean wind about its climatological

state, both with (e.g., Lorenz and Hartmann 2001, 2003; Chen and Plumb 2009; Byrne et al. 2016) and without (Ring and Plumb 2007, 2008; Lutsko et al. 2015; Hassanzadeh and Kuang 2016) vertical averaging. In the latter case, the validity of such a representation rests on a number of assumptions (Ring and Plumb 2008): that the mean flow is balanced, that variations of static stability are small, and that eddy feedback can be represented as a linear function of the instantaneous mean zonal wind anomaly. The latter assumption restricts the validity of (2) to time scales longer than those of baroclinic eddy life cycles (A. Sheshadri and R. A. Plumb 2016, unpublished manuscript).

The unforced system has modes described by the eigenvectors and eigenvalues of the operator **A**; if these are known, then the response to any forcing **f** can be determined. However, in practice **A** is not known, primarily because it includes the eddy feedback operator, a parameterization of which remains elusive. However the modes are implicit in the observed behavior of the system, which can be used to determine the eigenvectors of **A** in the form of the principal oscillation patterns. Assuming that the observed fluctuations of u are the responses of a stable system described by (2) to white-noise forcing, the eigenvectors of the matrix

$$\mathbf{G}(\tau) = \mathbf{C}(\tau)\mathbf{C}(0)^{-1}, \tag{3}$$

where

$$\mathbf{C}(\tau) = \mathrm{Cov}\{\mathbf{u}, \mathbf{u}; \tau\} = \mathbf{u}(x, t + \tau)\mathbf{u}^{\mathrm{T}}(x, t) \tag{4}$$
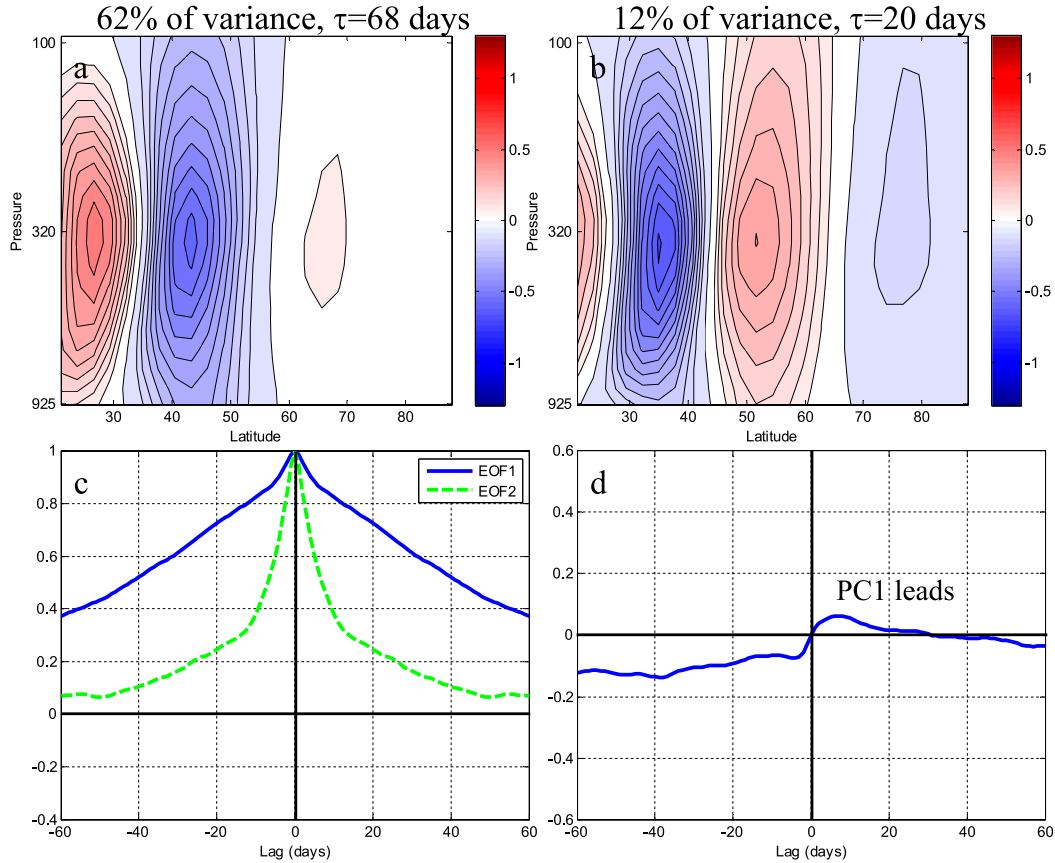
FIG. 6. As in Fig. 4, but for the summer hemisphere.

is the lag covariance of the zonal wind anomalies, are the eigenvectors of **A** (von Storch et al. 1988; Penland 1989). Thus, for a given lag τ, one can determine $\mathbf{G}(\tau)$ and hence its eigenvectors. In principle, the result of this process should be independent of lag; in practice this is true only to the extent that the theory is applicable at different lags. We shall show later that results, at least for this example, are quite robust to different choices of lag. The primary difficulty, however, arises from the need to invert $\mathbf{C}(0)$, which can be problematic. The inverse is dominated by those components with the smallest singular values—that is, those that contribute least to the variance (Martynov and Nechepurenko 2004). For this reason it has often been found expedient to improve the inversion by mapping the data onto a finite number of EOFs before applying (3) (e.g., Gritsun and Branstator 2007; Ring and Plumb 2008; Lutsko et al. 2015).

It is possible, however, to determine the POPs without the need to perform a matrix inversion by performing the calculations in EOF space, thereby diagonalizing the zero-lag covariance matrix (Penland 1989). Introducing the lag covariance of the normalized PCs

$$\hat{\mathbf{C}}(\tau) = \mathbf{V}_\tau^{\mathrm{T}}\mathbf{V}, \tag{5}$$

where the subscript τ denotes evaluation at lag τ, then (3), with (1) and (5), gives

$$\mathbf{G}(\tau) = \mathbf{U}\boldsymbol{\Sigma}\mathbf{V}_\tau^{\mathrm{T}}\mathbf{V}\boldsymbol{\Sigma}\mathbf{U}^{\mathrm{T}}\mathbf{U}\boldsymbol{\Sigma}^{-2}\mathbf{U}^{\mathrm{T}} = \mathbf{U}\boldsymbol{\Sigma}\hat{\mathbf{C}}(\tau)\boldsymbol{\Sigma}^{-1}\mathbf{U}^{\mathrm{T}}.$$

Therefore, introducing the eigenvector decomposition of $\hat{\mathbf{C}}(\tau)$,

$$\hat{\mathbf{C}}(\tau) = \mathbf{W}\boldsymbol{\Gamma}(\tau)\mathbf{W}^{-1}, \tag{6}$$

where $\boldsymbol{\Gamma}$ is the diagonal matrix of the eigenvalues, we have

$$\mathbf{G}(\tau) = \mathbf{U}\boldsymbol{\Sigma}\mathbf{W}\boldsymbol{\Gamma}(\tau)\mathbf{W}^{-1}\boldsymbol{\Sigma}^{-1}\mathbf{U}^{\mathrm{T}} = \mathbf{Z}\boldsymbol{\Gamma}(\tau)\mathbf{Z}^{-1}, \tag{7}$$

where the columns of the matrix

$$\mathbf{Z} = \mathbf{U}\boldsymbol{\Sigma}\mathbf{W} \tag{8}$$

are the POPs, the eigenvectors of $\mathbf{G}(\tau)$, and hence (von Storch et al. 1988; Penland 1989) of the system matrix.

The eigenvalues λ of $\mathbf{A}$ are not the same as those of $\mathbf{G}(\tau)$, but they are related through

$$\boldsymbol{\Gamma}(\tau) = \exp(-\boldsymbol{\Lambda}\tau), \qquad (9)$$

where $\boldsymbol{\Lambda}$ is the diagonal matrix with elements λ. Hence,

$$\mathbf{A} = \mathbf{Z}\boldsymbol{\Lambda}\mathbf{Z}^{-1}. \qquad (10)$$

Thus, taking this approach yields the POPs and their eigenvalues without the need to perform an explicit inversion of the covariance matrix and (as we shall see below) permits their evaluation without the need to truncate the data. One does need to invert $\boldsymbol{\Sigma}$ to obtain the inverses $\mathbf{Z}^{-1}$ (which are required to solve the inverse problem) but as one can obtain $\mathbf{W}^{-1}$ as the eigenvectors of $\hat{\mathbf{C}}^{\mathrm{T}}$, this only involves dividing by the singular values, rather than by the square of the singular values and the procedure is thus less ill conditioned.

One advantage of POPs over EOFs is that the latter are dependent on how the data are weighted before applying (1), whereas it is straightforward to show that the POPs are independent of such weighting (appendix A). (This is no longer true if one uses a truncated series of EOFs to filter the data.) This fact can become especially important for a deep system (such as the troposphere and stratosphere) if, say, pressure weighting is applied.

In general, since $\mathbf{G}(\tau)$ is real, either its eigenvalues are real, with real eigenvectors, or they appear as conjugate pairs with conjugate eigenvectors. If the PCs are mutually independent (i.e., their cross covariances are zero at all lags), then

$$\hat{C}_{mn}(\tau) = \begin{cases} 0, & m \neq n \\ \hat{C}_{mm}(\tau), & m = n \end{cases}$$

and the eigenvalues of $\hat{\mathbf{C}}(\tau)$, and hence of $\mathbf{G}(\tau)$, are just the PC autocovariances $\hat{C}_{mm}(\tau)$; if $\hat{C}_{mm} = \exp(-\alpha_m \tau)$ (so that the decorrelation time of each PC is just α_m^{-1}) then, by (9), the eigenvalues of $\mathbf{A}$ are just $\lambda_m = \alpha_m$. Further, the POPs Z are the same as the EOFs. In such a case, therefore, the EOFs and the PC decorrelation rates describe the modes of the system. Clearly, however, this is not generally true of a system in which the PCs have nonzero cross correlations, as we shall now illustrate, using results from the dry dynamical core model.

b. POPs in the dynamical core model

Following the outlined procedure, the POPs were calculated for the winter and summer hemispheres. It is first necessary to choose a value of lag τ at which to evaluate the PC lag covariances. For reasons noted above, it is desirable to avoid short lags ($\tau < 10$ days); lags much longer than one decorrelation time scale are also best avoided, as the correlations then become weak. Accordingly, the calculation was done for $\tau = 20$ days for the winter hemisphere and $\tau = 60$ days for summer. (Robustness of the results with respect to the chosen lag will be discussed below.)

One further consideration concerns selection of the POPs (of many) that are of interest. For the EOFs, the association of their singular values with variance explained lends itself to a natural (and conventional) ranking by decreasing variance. No such obvious ranking exists for the POPs; their eigenvalues determine the time scales for each mode but bear no direct relationship to explained variance.[2] Since it is the two leading EOFs that, by definition, explain the most variance, we focus attention here on those POPs onto which the first two EOFs project the most strongly.

The resulting POPs, and their eigenvalues, form a complex conjugate pair. The real and imaginary parts of the POPs $Z(\varphi, p)$ and $Z^*(\varphi, p)$ are shown in Fig. 7. In the winter case, $\mathrm{Re}(Z)$ and $\mathrm{Im}(Z)$ strongly reflect the structure of the EOFs, with only minor differences. The corresponding eigenvalues are $\lambda = \lambda_R + i\lambda_I = 0.0256 \pm 0.0467i\,\mathrm{day}^{-1}$. Each of the conjugate pair of modes has space–time structure

$$Z(\varphi, p) \exp(-\lambda_R t) \exp(i\lambda_I t)$$
$$= \{\mathrm{Re}[Z(\phi, p)]\cos\lambda_I t - \mathrm{Im}[Z(\phi, p)]\sin\lambda_I t\} \exp(-\lambda_R t)$$

and thus describes a propagating decaying disturbance. The time scale for decay is $\lambda_R^{-1} = 39$ days and the period of oscillation $2\pi\lambda_I^{-1} = 135$ days; these do not appear to correspond well to the PC decorrelation times of 19 and 13 days, but it will be shown below that they are, in fact, mutually consistent.

The summer case, on the other hand, is more straightforward. The real part of Z is almost identical to EOF1, while its imaginary part is very small. Similarly, its corresponding eigenvalue $\lambda = 0.0134 \pm 0.0033i\,\mathrm{day}^{-1}$ is dominated by its real part. To a first approximation, then, this mode describes a decaying disturbance, with very weak propagation and decay time $\lambda_R^{-1} = 75$ days, not very different from the PC decorrelation time of 68 days. This reinforces the suggestion made above that when lagged cross correlations between PCs are weak, POPs and EOFs are essentially identical.

The robustness of the calculation to chosen lag τ for evaluation of the cross correlation is illustrated in Fig. 8, which shows how the eigenvalue λ for the propagating

---

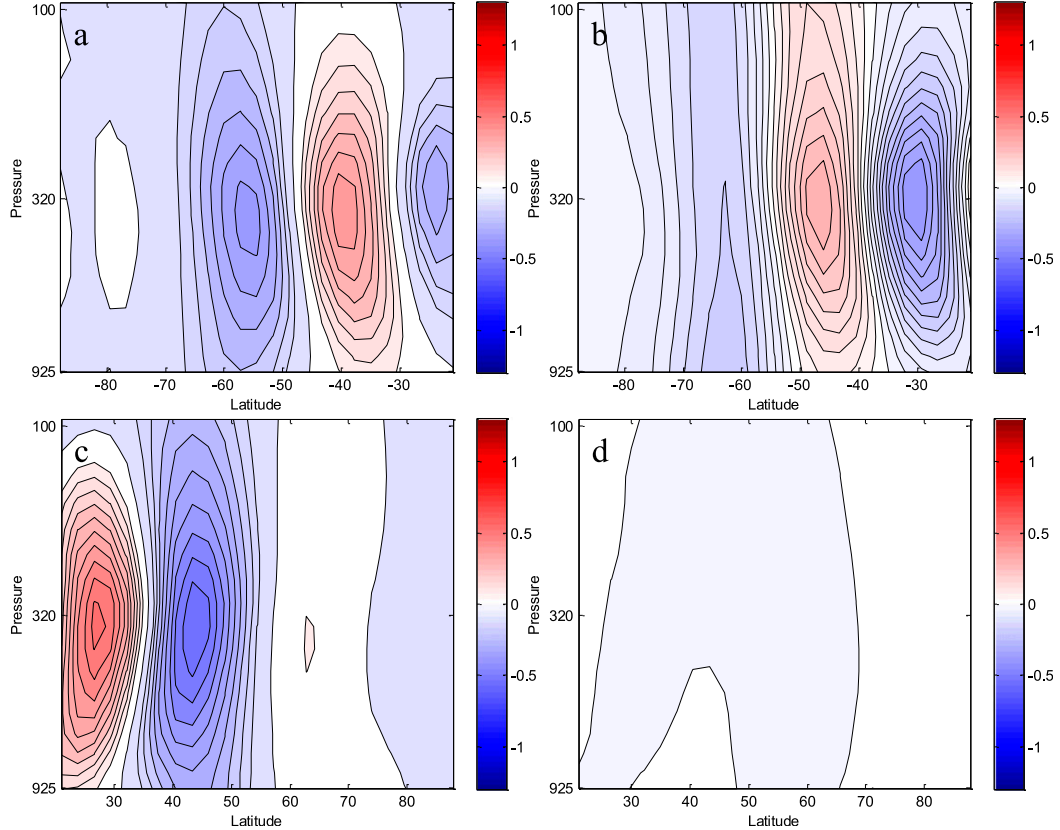[2] A methodology for ascribing variance explained to the POPs has been outlined in Gallagher et al. (1991).

FIG. 7. Principal oscillation patterns determined separately for each hemisphere from zonal wind data poleward of 20°S. (a) Real and (b) imaginary parts of the dominant winter hemisphere POP calculated at 20-day lag and chosen as described in the text. The corresponding eigenvalue is $\lambda = 0.0256 \pm 0.0467i\,\text{day}^{-1}$. (c) Real and (d) imaginary parts of the dominant summer hemisphere POP calculated at 60-day lag and chosen as described in the text. The corresponding eigenvalue is $\lambda = 0.0134 \pm 0.0033i\,\text{day}^{-1}$.

case depends on τ. While there is some sensitivity, there is a wide range of lags $20 \leq \tau \leq 50$ days over which the eigenvalue changes little. (The calculation becomes problematic near $\tau = 60$ days, where the cross correlations pass through zero.)

5. Lag covariances under stochastic forcing

a. Covariances of the POP coefficients

Once the eigenvectors and eigenvalues have been determined from (8) for a given lag $\tau = \tau_0$, (6) can then be used to predict the covariances at other lags, under the assumption that the variability is the response to white-noise forcing. Then, as noted above and expressed by (9), $\mathbf{\Gamma}(\tau)$ varies exponentially with lag, and therefore the PC covariances become

$$\hat{\mathbf{C}}(\tau) = \mathbf{W}[\mathbf{\Gamma}(\tau_0)]^{\tau/\tau_0}\mathbf{W}^{-1} \qquad (11)$$

(Penland 1989). For the two PCs of major interest, then,

$$\hat{C}_{mn}(\tau) = \sum_{p=1}^{N} W_{mp}\gamma_p^{\tau/\tau_0}(W^{-1})_{pn}, \qquad (12)$$

where $m, n = 1$ or 2, N is the total number of modes, and γ_p is the pth element of the diagonal matrix $\mathbf{\Gamma}(\tau_0)$.

Given the dominance of PC1 and PC2 (explaining 69% of the variance between them) and the finding that to a good approximation they are encapsulated in a single conjugate pair of POPs (whose eigenvectors and eigenvalues are mutual complex conjugates), it is instructive to truncate to these two modes by terminating the sum in (12) at $N = 2$, in which case we have

$$\hat{C}_{mn}(\tau) = W_{m1}\gamma_1^{\tau/\tau_0}(W^{-1})_{p1} + \text{c.c.}, \qquad (13)$$

where "c.c." denotes complex conjugate. Then it is shown in appendix B that the autocorrelations are

$$\hat{C}_{11}(\tau) = \frac{\cos(\lambda_I|\tau| + \chi)}{\cos\chi}\exp(\lambda_R|\tau|) \quad \text{and} \quad (14)$$
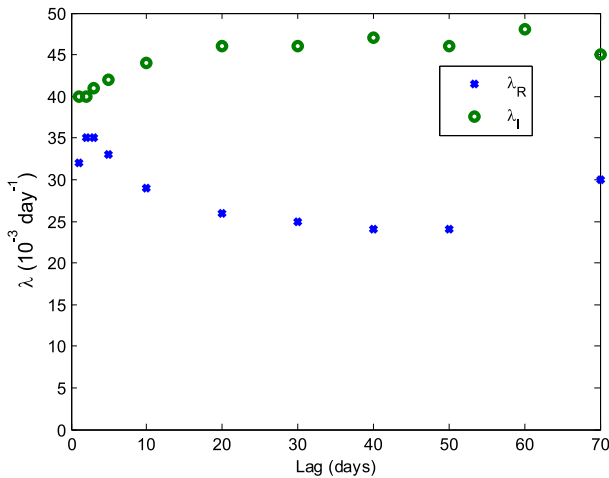
FIG. 8. Dependence of the calculated eigenvalue $\lambda = \lambda_R + i\lambda_I$ on the choice of lag τ.

$$\hat{C}_{22}(\tau) = \frac{\cos(\lambda_I|\tau| - \chi)}{\cos\chi}\exp(\lambda_R|\tau|), \qquad (15)$$

and the cross correlation is

$$\hat{C}_{12}(\tau) = \begin{cases} \dfrac{|W_{12}|^2}{\operatorname{Im}(W_{11}W_{12}^*)}\sin(\lambda_I\tau)\exp(\lambda_R|\tau|); & \tau < 0 \\[3mm] -\dfrac{|W_{11}|^2}{\operatorname{Im}(W_{11}W_{12}^*)}\sin(\lambda_I\tau)\exp(\lambda_R|\tau|); & \tau > 0 \end{cases}, \qquad (16)$$

where $\chi = \arg(-iW_{11}W_{12}^*)$ and

$$\lambda_1 = \lambda_R + i\lambda_I = \tau_0^{-1}\ln\gamma_1, \qquad (17)$$

where λ_R and λ_I are real.

Several points of interest become evident from (14)–(16). First, the decay of the autocorrelations is not exponential, except in the limit of a single uncoupled mode for which $\lambda_I = 0$. Second, the two autocorrelations have different dependencies on lag, despite the fact that they are manifestations of the same mode. Third, the cross correlation is asymmetric: the coefficients in (16) differ for positive and negative τ. We shall now assess the impact of these characteristics on the example from the model's winter hemisphere.

b. Application to model data

For the propagating case of the model's winter hemisphere discussed in sections 3 and 4 and shown in Figs. 4 and 7, reconstructed lag correlations of the PCs given by (11) are shown in Figs. 9a and 9b. The separation of the two PC autocorrelations is noticeable, as is the asymmetry of the cross correlation. Comparing these

predictions with the PC lag correlations determined from the model and shown in Fig. 4, the similarity is obvious. It should be noted that although there is some circularity in this comparison—the coefficients were themselves derived from the model results—all the information was obtained from the PC covariances at a single lag: the lag dependence shown in Fig. 9 derives entirely from the theoretical analysis.

Lag correlations calculated from the truncated results given in (14)–(16) are shown in Figs. 9c and 9d. Agreement with the model results shown in Figs. 4c and 4d is now more qualitative. Nevertheless, from (14) and (15) and Fig. 9c, the more rapid decay of PC2 compared with PC1 evident in Fig. 4c and in its shorter "decorrelation time" can now be seen as a consequence of the propagation of the mode. Although the decay time of the mode λ_R^{-1} is 39 days, the autocorrelations decay much more rapidly, because of the trigonometric terms in (16). Thus, the loss of correlation is as much a consequence of propagation—P_1 becoming P_2 and vice versa—as of true decay of the mode. Indeed, the autocorrelations change sign at lags of 42 and 31 days. There are discrepancies: it has already been noted that the assumption of white-noise forcing renders the results inapplicable at short lags, and the timing of the zero crossings is not quite correct. Nevertheless, it seems clear that the fact that we are here dealing with a propagating mode is the basic reason for the separation of the PC autocorrelations seen in the model output.

The cross correlations determined from the truncated result in (16), while qualitatively satisfactory, are too large in magnitude [as compared with the model results of Fig. 4d and with the untruncated theoretical prediction of (11) and Fig. 9b] by a factor of about 1.7. The discrepancies between the truncated and untruncated results indicate that, despite some indications to the contrary, contributions to the leading mode from EOFs other than the first two are not quantitatively negligible.

c. Implications for the climate perturbation problem

Finally, we note the implications of these results for the "climate" problem of the system response to steady, weak, imposed forcing. Solution of (2) for such a case requires inversion of the operator $\mathbf{A}$; assuming Gaussian PDFs of the variability, the fluctuation–dissipation theorem (Leith 1975; North et al. 1993; Majda et al. 2005; Gritsun and Branstator 2007) states that

$$\mathbf{L} = \mathbf{A}^{-1} = \int_0^\infty \mathbf{G}(\tau)\,d\tau,$$

where $\mathbf{G}(\tau)$ was defined in (3). Using our formulation (7) with (9), this becomes simply
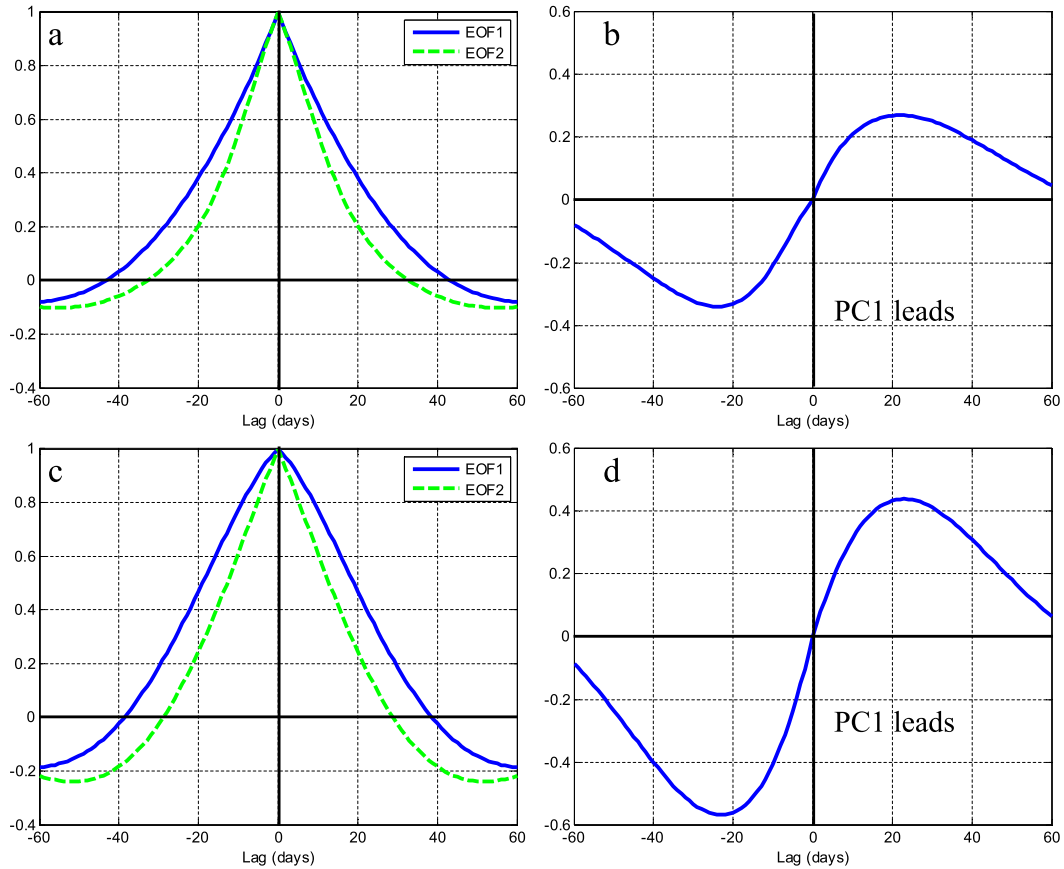
FIG. 9. Predicted lag correlations of the PCs using parameters from the model results at a lag of 20 days. (a) Autocorrelations of P_1 (solid) and P_2 (dashed). (b) Lag correlation of P_1 and P_2. (c) Autocorrelations and (d) cross correlation after truncating the series in (12) to $N = 2$.

$$\mathbf{L} = \mathbf{Z}\boldsymbol{\Lambda}^{-1}\mathbf{Z}^{-1}. \qquad (18)$$

For the steady response to steady forcing in (2), the zonal wind response in each POP mode becomes

$$\mathbf{Z}^{-1}\mathbf{u} = \boldsymbol{\Lambda}^{-1}\mathbf{Z}^{-1}\mathbf{f} \qquad (19)$$

(i.e., simply the projection $\mathbf{Z}^{-1}\mathbf{f}$ of the forcing onto the POPs divided by the corresponding eigenvalue). [Note, following Ring and Plumb (2008) and Lutsko et al. (2015), that $\mathbf{f}$ is not just the imposed forcing that appears in the momentum equation but is the "Eliassen response" of the zonal wind tendency to any imposed mechanical or thermal forcing.]

Interpretation of (19) is confounded somewhat by the fact that the POPs Z and their eigenvalues λ are complex. The relationship can also be expressed in terms of the projection of the response and forcing onto the EOFs U, using (8) to give

$$\mathbf{U}^{\mathrm{T}}\mathbf{u} = \mathbf{D}\mathbf{U}^{\mathrm{T}}\mathbf{f}, \qquad (20)$$

where

$$\mathbf{D} = \boldsymbol{\Sigma}\mathbf{W}\boldsymbol{\Lambda}^{-1}\mathbf{W}^{-1}\boldsymbol{\Sigma}^{-1}. \qquad (21)$$

As discussed earlier, in circumstances in which the PCs are all independent, the POPs are just the EOFs, the eigenvalues are real and equal to the inverse of the PC decorrelation time, and $\mathbf{W}$ is diagonal, so that $\mathbf{D} = \boldsymbol{\Lambda}^{-1}$ is also diagonal. Then if we write the projection of response and forcing onto the nth EOF as $u_n = (\mathbf{U}^{\mathrm{T}}\mathbf{u})_n$ and $g_n = (\mathbf{U}^{\mathrm{T}}\mathbf{f})_n$, we have $u_n = \lambda_n^{-1}g_n$, and thus the response in the leading mode depends on the projection of the forcing onto the EOF, multiplied by a time scale given by the corresponding PC decorrelation time (Ring and Plumb 2008). Thus, for example, if the forcing projects equally onto all EOFs, response is favored in the EOF corresponding to the longest decorrelation time (Gerber et al. 2008; Ring and Plumb 2008).

In the more general case, however, including the propagating regime, $\mathbf{D}$ is not diagonal, implying that the response in a given EOF does not depend solely on
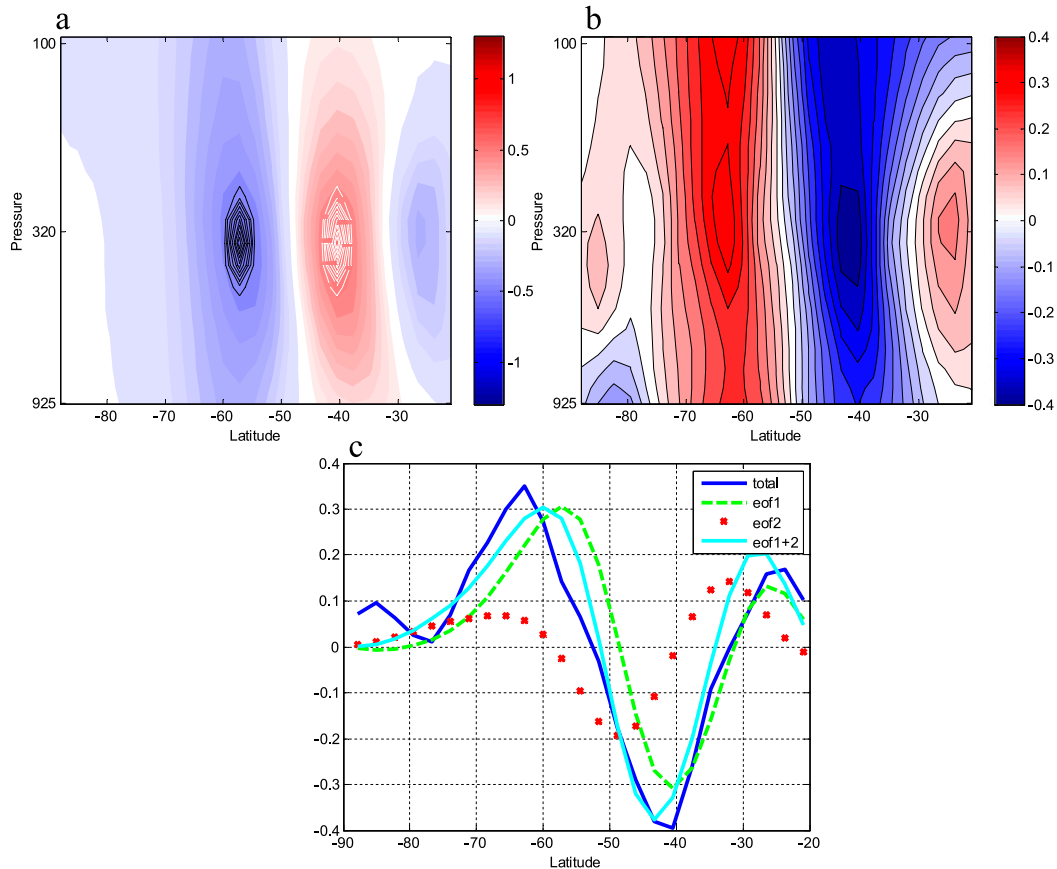
FIG. 10. (a) The shape of the imposed torque (black and white contours indicate positive and negative values, respectively), superimposed on the latitude–pressure structure of EOF1, (b) the zonal-mean zonal wind response to the imposed torque, and (c) the zonal wind response at 340 hPa (solid blue line), the EOF1 component of this response (dashed green line), the EOF2 component of this response (red crosses), and the sum of the EOF1 and EOF2 components (solid cyan line).

the projection of the forcing onto that EOF. For the 2×2 problem, in which we truncate to the two leading EOFs and the corresponding two, mutually conjugate, POPs, it can be shown that

$$\mathbf{D} = \begin{pmatrix} D_{11} & D_{12} \\ D_{21} & D_{22} \end{pmatrix}$$
$$= [|\lambda|^2 \mathrm{Re}(\mu)]^{-1} \begin{bmatrix} \mathrm{Re}(\mu\lambda) & -\mathrm{Im}(\lambda) \\ |\mu|^2 \mathrm{Im}(\lambda) & \mathrm{Re}(\mu\lambda*) \end{bmatrix}, \quad (22)$$

where μ is defined in appendix B. Hence there is cross fertilization—a nonzero response in EOF2 (EOF1) to a forcing purely in EOF1 (EOF2)—whenever $\mathrm{Im}(\lambda) \neq 0$ (i.e., whenever there is propagation). We illustrate this by forcing the dynamical core model with a steady localized torque. The torque is Gaussian in latitude and in the model's vertical coordinate, peaking at 340 hPa and at the peaks of EOF1 at this pressure level; the shape of the torque is indicated in the black and white contours in

Fig. 10a. The response, shown in Fig. 10b, is dipolar, but does not exactly match the latitudinal structure of EOF1. Much of this discrepancy can be explained by the component of the response explained by EOF2 (Fig. 10c), resulting in a poleward shift of the response with respect to EOF1, and demonstrating that a forcing designed to match the structure of EOF1 results in a substantial response in EOF2. Note that there is no differential selectivity of EOF1 versus EOF2 responses based on their decorrelation times, which do not appear separately in the problem.

6. Propagation in Southern Hemisphere data

In this section, we investigate the applicability of the model behavior to observations of the Southern Hemisphere zonal flow. We use daily data from the ERA-Interim (Dee et al. 2011) for the years 1979–2013 on 21 vertical levels between 1000 and 100 hPa. Examples of the evolution of zonal-mean zonal wind anomalies were
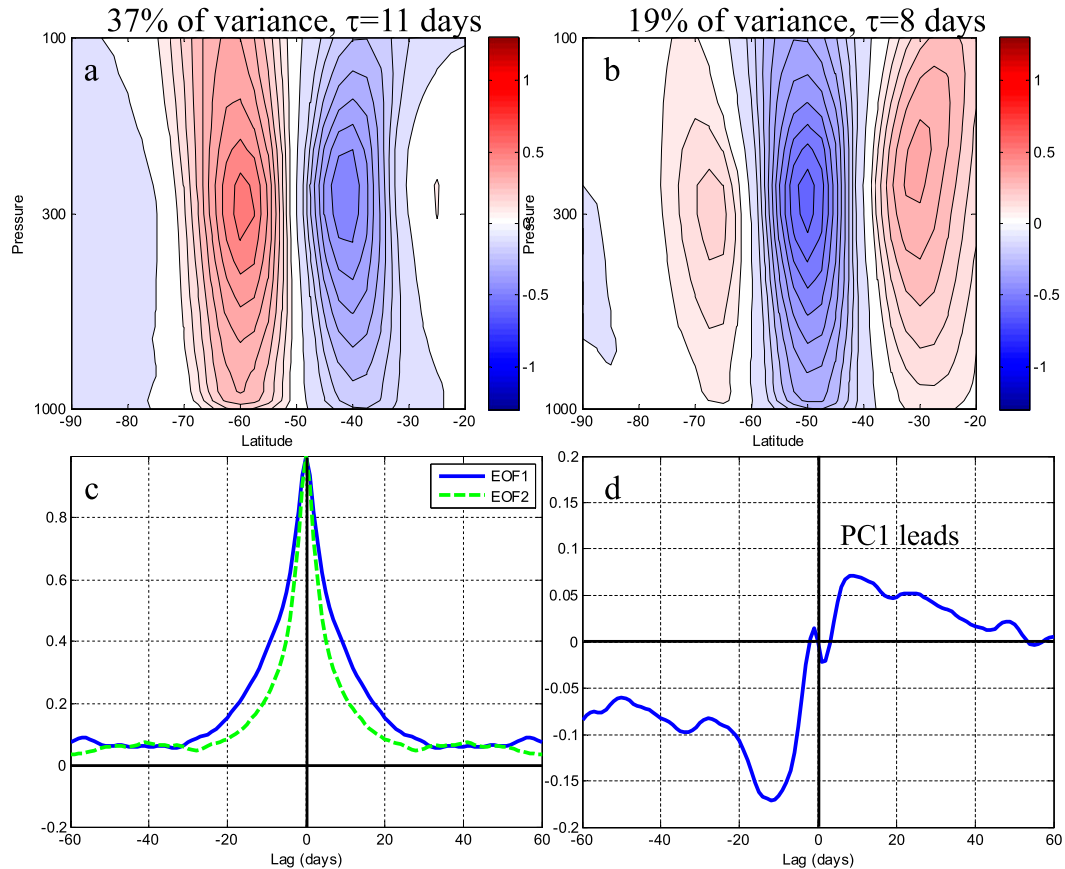
FIG. 11. As in Fig. 4 (the two leading EOFs of zonal-mean zonal wind), but for the observed Southern Hemisphere, calculated from ERA-Interim.

shown in Fig. 1. As with the model analysis in section 2, we consider fluctuations of zonal-mean zonal wind poleward of 20°S, over the entire record (i.e., including all seasons). The first two EOFs of zonal-mean zonal wind are shown in Fig. 11. These two leading EOFs contribute 37% and 19%, respectively, to the total variance and have decorrelation times of 11 and 8 days. Figure 11 also shows the PC auto- and cross correlations associated with these two EOFs. Note that the autocorrelations appear to asymptotically approach a nonzero positive value at large lag, which may indicate the influence of interannual variability (Keeley et al. 2009; Byrne et al. 2016). As in the winter hemisphere in the idealized model, the two PCs show some cross correlation peaking near 12 days, but with smaller magnitudes. The POPs were calculated and chosen based on the procedure outlined in section 4a, with the PC covariances calculated at $\tau = 10$ days (similar to the decorrelation time of the first PC). The results (Fig. 12) bear a strong resemblance to those of the model's winter hemisphere, with the real and imaginary parts of the POP primarily reflecting the structures of EOFs 1 and 2 (Fig. 11). The corresponding eigenvalues

are $\lambda = 0.0902 \pm 0.0346i\,\mathrm{day}^{-1}$ (which imply a decay time scale of 11.1 days and a period of oscillation of 182 days). Figure 13 shows the auto- and cross correlations calculated using (11) in Figs. 13a and 13b and the truncated results [see (14)–(16)] shown in Figs. 13c and 13d. There is good agreement between the correlations shown in Fig. 11 and the untruncated results, with differences at the detailed level. As for the model results shown earlier, the truncated theory is less successful at reproducing the observed lag correlations. However, poleward propagation of zonal-mean zonal wind anomalies is not always evident in observations of Southern Hemisphere winds, as was shown in Fig. 1. In fact, since the ratio of variance contributions of EOF1 and EOF2 is close to 2, this propagating/nonpropagating behavior is consistent with the criterion of Son and Lee (2006), for which a ratio of 2 is marginal.

7. Discussion and conclusions

These theoretical and modeling results have several implications for our understanding of annular modes
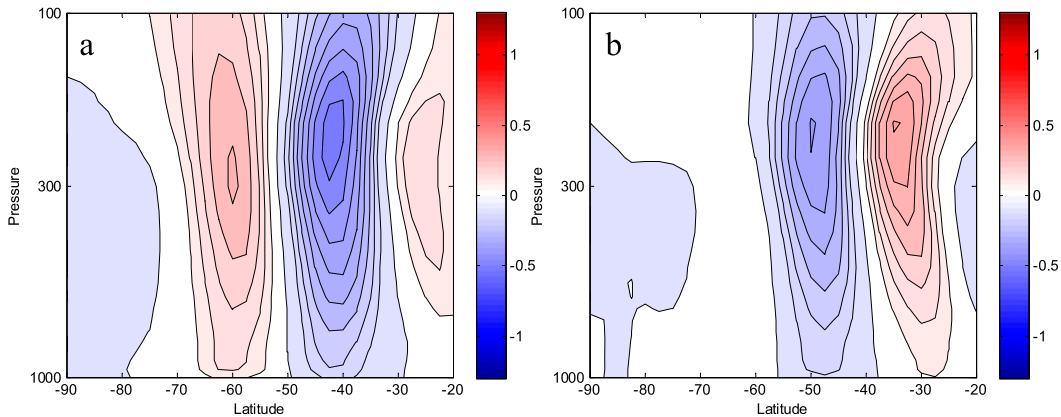
FIG. 12. Principal oscillation patterns for the observed Southern Hemisphere, calculated from ERA-Interim. (a) Real and (b) imaginary parts of the dominant winter hemisphere POP calculated at 10-day lag, and chosen as described in the text. The corresponding eigenvalue is $\lambda = 0.0902 \pm 0.0346i\,\mathrm{day}^{-1}$.

and their role in climate variability. Perhaps the most important conclusion is that whenever the leading mode is propagating (revealed by finite lag correlations between the two leading PCs) one cannot regard the two leading EOFs as being independent; rather, they are simply two projections into EOF space of a single mode [as is made clear by the analyses of Son and Lee (2006) and Sparrow et al. (2009) and by the fact that the
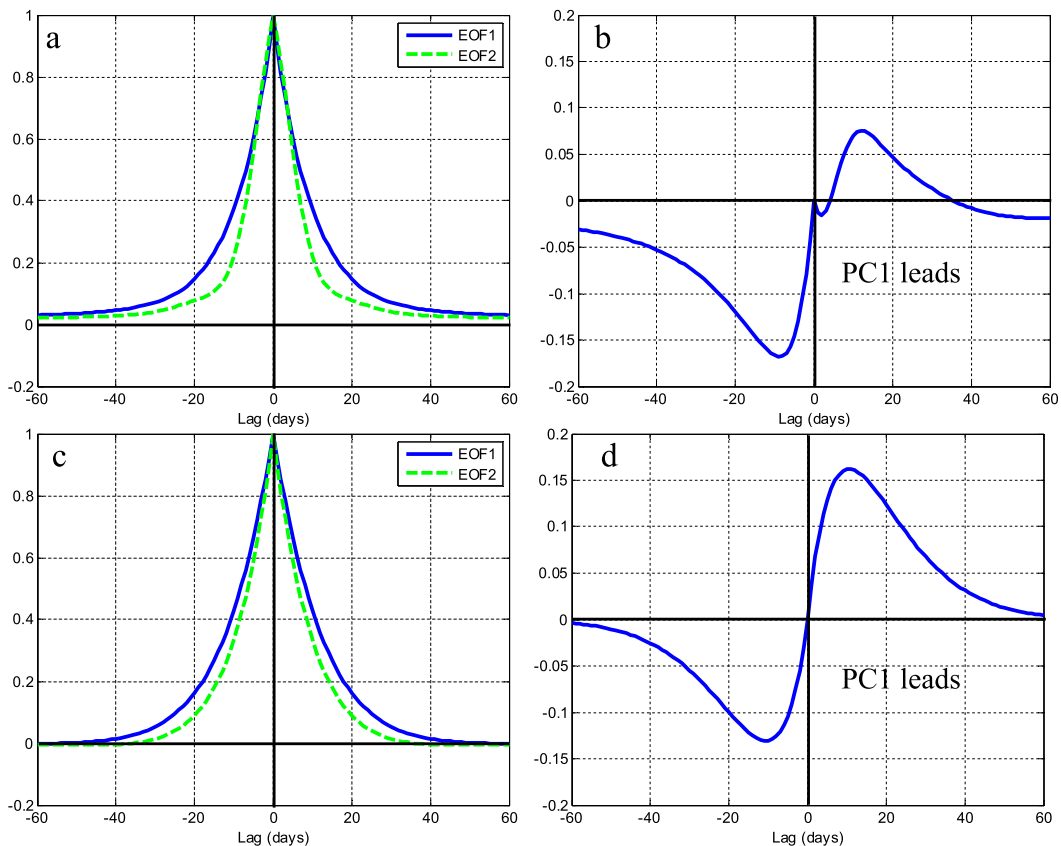

FIG. 13. Predicted lag correlations of the PCs using parameters from the ERA-Interim results at a lag of 20 days. (a) Autocorrelations of P_1 (solid) and P_2 (dashed). (b) Lag correlation of P_1 and P_2. (c) Autocorrelations and (d) cross correlation after truncating the series in (12) to $N = 2$.

corresponding POPs form a conjugate pair]. Propagation is not just a characteristic of this kind of model; Feldstein (1998) described poleward-propagating zonal wind anomalies in both hemispheres (Southern Hemisphere propagation was also shown in Fig. 1 here), and Lorenz and Hartmann (2001) noted that the characteristics of the two leading Southern Hemisphere PCs are consistent with propagation. Reasons for the propagation are not addressed here; Robinson (1994, 2000) and Lee et al. (2007) have described how the eddy flux response to zonal wind anomalies can lead to poleward propagation in the atmosphere, while Chan et al. (2007) have described similar processes leading to equatorward propagation in a simple ocean model.

One important consequence of the propagation is that the PC autocorrelations decay nonexponentially and faster than the mode itself decays. In the winter example discussed here, the apparent decorrelation time, obtained by fitting an exponential to the PC1 autocorrelation function, of 19 days is much shorter than the POP decay time of 39 days. Since the persistence of the mode, beyond time scales of dissipation by surface drag, can be taken as indicative of eddy feedback acting to maintain the anomalous winds, it follows that the eddy feedback may be underestimated if the PC decorrelation time is interpreted as the relevant decay time (e.g., Chen and Plumb 2009). A second consequence is that the autocorrelation functions of the two leading PCs separate and have different apparent decorrelation times. Lorenz and Hartmann (2001) interpreted such a separation between the PCs corresponding to the two leading Southern Hemisphere EOFs as indicative of eddy feedback acting on EOF1 but not EOF2, an interpretation that clearly would not be valid in the winter case analyzed here. In a propagating regime, decay of the autocorrelations occurs through conversion between PCs, and not just dissipation of the mode. Moreover, since the two modes share a conjugate pair of eigenvalues, they must be subject to the same eddy feedback strength.

Analysis of Southern Hemisphere winds from ERA-Interim produces results that are consistent with the propagating regime in the winter hemisphere of the dynamical core model: the two leading EOFs are manifestations of a single dynamical mode with complex conjugate eigenvectors and eigenvalues. Poleward propagation of zonal-mean zonal wind anomalies is clearly evident in reanalysis data and is not obviously confined to any given season, but unlike in the propagating regime in the idealized model, this feature is not ubiquitous, consistent with the criterion of Son and Lee (2006), which, given the ratio of variances explained by EOFs 1 and 2, places the observed Southern Hemisphere as marginal for propagation, at least over the multiyear and all-season average used here.

Finally, we note that the "climate" problem of the steady response to anomalous steady forcing is more complex in the propagating regime than in the nonpropagating case. For the nonpropagating case with a single dominant EOF, the eigenvalue λ is just the inverse of the decorrelation time of the primary PC, and thus the response in the leading mode depends on the projection of the forcing onto the EOF, multiplied by a time scale given by the PC decorrelation time. In such a regime, Ring and Plumb (2008) found some success, though with quantitative limitations, applying (18) to a model similar to that used here, and using the PC decorrelation time as the time scale. Nevertheless, it is clear that, in the propagating regime, the relevant time scale may differ significantly from the PC decorrelation time (as is the case in the example analyzed here). Moreover, since the leading mode comprises (at least) two EOFs, a forcing that projects purely onto EOF1 will produce a response in EOF2 as well as EOF1, and vice versa. We note that this might explain the findings of Black et al. (2006) and Black and McDaniel (2007), from Northern and Southern Hemisphere observations, and Sheshadri et al. (2014), from a dynamical core model, that the tropospheric response to the stratospheric final warming does not project very well onto the leading EOF of zonal wind variability. In particular, responses are likely to project onto at least two EOFs [this is consistent with Sheshadri and Plumb (2016), who found that the tropospheric response to lower-stratospheric cooling in a very similar idealized model as is used here contained a substantial contribution from EOF2, in addition to EOF1]. Further, the coefficient that determines the sensitivity of the system is not just the decorrelation time of the leading PC, but involves at least two time scales: that governing the rate of decay of the dynamical mode and the period associated with the propagation.

their constructive comments, which greatly improved the manuscript.

APPENDIX A

Independence of POPs under Weighting

If the variable $\mathbf{X}$ is weighted, $\tilde{\mathbf{X}} = \mathbf{\Omega}\mathbf{X}$, the covariances in weighted space are

$$\tilde{\mathbf{C}}_\tau = \tilde{\mathbf{X}}_0 \tilde{\mathbf{X}}_\tau^T = \mathbf{\Omega}\mathbf{X}_0 (\mathbf{\Omega}\mathbf{X}_\tau)^T = \mathbf{\Omega}\mathbf{X}_0 \mathbf{X}_\tau^T \mathbf{\Omega} = \mathbf{\Omega}\mathbf{C}_\tau \mathbf{\Omega},$$

where $\mathbf{\Omega}$ is the diagonal matrix of weights. Then

$$\tilde{\mathbf{C}}_0^{-1} = (\mathbf{\Omega}\mathbf{C}_0\mathbf{\Omega})^{-1} = \mathbf{\Omega}^{-1}\mathbf{C}_0^{-1}\mathbf{\Omega}^{-1}.$$

So,

$$\tilde{\mathbf{G}}_\tau = \tilde{\mathbf{C}}_\tau \tilde{\mathbf{C}}_0^{-1} = \mathbf{\Omega}\mathbf{C}_\tau \mathbf{\Omega}\mathbf{\Omega}^{-1} \mathbf{C}_0^{-1}\mathbf{\Omega}^{-1} = \mathbf{\Omega}\mathbf{G}_\tau \mathbf{\Omega}^{-1}.$$

Hence, $\tilde{\mathbf{G}}_\tau = (\mathbf{\Omega}\mathbf{W})\mathbf{\Gamma}(\mathbf{\Omega}\mathbf{W})^{-1}$.

So the eigenvalues are the same, and the deweighted eigenvectors $\mathbf{\Omega}^{-1}(\mathbf{\Omega}\mathbf{W}) = \mathbf{W}$ are also the same as in the unweighted case.

APPENDIX B

Covariances When Truncated to Two Modes and Two EOFs

If the two EOFs of interest are $U_1(\varphi, p)$ and $U_2(\varphi, p)$, and the two corresponding truncated POPs are $Z_1(\varphi, p)$ and $Z_2(\varphi, p) = Z_1^*(\varphi, p)$, with eigenvalues $\lambda_1 = \lambda_2^* = \lambda$, then

$$Z_1 = U_1 \sigma_1 W_{11} + U_2 \sigma_2 W_{21} \quad \text{and}$$
$$Z_2 = U_1 \sigma_1 W_{12} + U_2 \sigma_2 W_{22},$$

where $W_{12} = W_{11}^*$ and $W_{22} = W_{21}^*$. Defining $\mathbf{R}^T = \mathbf{W}^{-1}$, then

$$\begin{pmatrix} R_{11} & R_{12} \\ R_{21} & R_{22} \end{pmatrix} = \frac{1}{(W_{11}W_{21}^* - W_{11}^* W_{21})} \times \begin{pmatrix} W_{21}^* & -W_{21} \\ -W_{11}^* & W_{11} \end{pmatrix}.$$

Since the only independent coefficients are W_{11} and W_{12}, we can simplify the algebra by defining μ such that $W_{21} = \mu^* W_{11}$; then, using (15) and (11),

$$\hat{C}_{11}(\tau) = \left(\frac{\mu}{\mu - \mu^*}\right) e^{\lambda\tau} + \text{c.c.}, \quad \tau > 0,$$

where "c.c." denotes complex conjugate. If we define $\chi = \arg(-i\mu)$, then

$$\left(\frac{\mu}{\mu - \mu^*}\right) = \frac{1}{2} \frac{e^{i\chi}}{\cos\chi},$$

whence $\hat{C}_{11}(\tau) = [\cos(\lambda_I \tau + \chi)/\cos\chi]e^{\lambda_R\tau}, \quad \tau > 0$.
Therefore, since $\hat{C}_{11}(-\tau) = \hat{C}_{11}(\tau)$,

$$\hat{C}_{11}(\tau) = \frac{\cos(\lambda_I|\tau| + \chi)}{\cos\chi} e^{\lambda_R|\tau|}, \quad \forall\tau.$$

Similarly, we find

$$\hat{C}_{22}(\tau) = \frac{\cos(\lambda_I|\tau| - \chi)}{\cos\chi} e^{\lambda_R|\tau|}, \quad \forall\tau.$$

The cross correlations are, for $\tau > 0$,

$$\hat{C}_{12}(\tau) = -\frac{1}{\text{Im}(\mu)} e^{\lambda_R\tau} \sin\lambda_I\tau, \quad \tau > 0 \quad \text{and}$$

$$\hat{C}_{21}(\tau) = \frac{|\mu|^2}{\text{Im}(\mu)} e^{\lambda_R\tau} \sin\lambda_I\tau, \quad \tau > 0.$$

Since $\hat{C}_{12}(-\tau) = \hat{C}_{21}(\tau)$, it follows that

$$\hat{C}_{12}(\tau) = -\frac{|\mu|^2}{\text{Im}(\mu)} e^{\lambda_R|\tau|} \sin\lambda_I\tau, \quad \tau < 0 \quad \text{and}$$

$$\hat{C}_{21}(\tau) = \frac{1}{\text{Im}(\mu)} e^{\lambda_R|\tau|} \sin\lambda_I\tau, \quad \tau < 0.$$

REFERENCES

Black, R. X., and B. A. McDaniel, 2007: Interannual variability in the Southern Hemisphere circulation organized by stratospheric final warming events. *J. Atmos. Sci.*, **64**, 2968–2974, doi:10.1175/JAS3979.1.

——, ——, and W. A. Robinson, 2006: Stratosphere–troposphere coupling during spring onset. *J. Climate*, **19**, 4891–4901, doi:10.1175/JCLI3907.1.

Byrne, N., T. G. Shepherd, T. Woolings, and R. A. Plumb, 2016: Annular modes and apparent eddy feedbacks in the Southern Hemisphere. *Geophys. Res. Lett.*, **43**, 3897–3902, doi:10.1002/2016GL068851.

Chan, C. J., and R. A. Plumb, 2009: The response of the troposphere to stratospheric perturbations and its dependence on the state of the troposphere. *J. Atmos. Sci.*, **66**, 2107–2115, doi:10.1175/2009JAS2937.1.

——, I. Cerovecki, and R. A. Plumb, 2007: Annular modes in a migrating zonal jet regime. *J. Atmos. Sci.*, **64**, 4053–4068, doi:10.1175/2007JAS2156.1.

Chen, G., and R. A. Plumb, 2009: Quantifying the eddy feedback and the persistence of the zonal index in an idealized atmospheric model. *J. Atmos. Sci.*, **66**, 3707–3720, doi:10.1175/2009JAS3165.1.

Dee, D. P., and Coauthors, 2011: The ERA-Interim reanalysis: Configuration and performance of the data assimilation system. *Quart. J. Roy. Meteor. Soc.*, **137**, 553–597, doi:10.1002/qj.828.

Feldstein, S. B., 1998: An observational study of the intraseasonal poleward propagation of zonal mean flow anomalies. *J. Atmos.*

Sci., **55**, 2516–2529, doi:10.1175/1520-0469(1998)055<2516: AOSOTI>2.0.CO;2.

Gallagher, F., H. von Storch, R. Schnur, and G. Hannoschöck, 1991: The POP manual. Deutches KlimaRechenZentrum Tech. Rep. 1, 64 pp. [Available online at http://www.hvonstorch.de/klima/pdf/POP-manual.dkrz.1991.pdf.]

Gerber, E. P., S. Voronin, and L. M. Polvani, 2008: Testing the annular mode autocorrelation time scale in simple atmospheric general circulation models. *Mon. Wea. Rev.*, **136**, 1523–1536, doi:10.1175/2007MWR2211.1.

Gritsun, A., and G. Branstator, 2007: Climate response using a three-dimensional operator based on the fluctuation–dissipation theorem. *J. Atmos. Sci.*, **64**, 2558–2575, doi:10.1175/JAS3943.1.

Hassanzadeh, P., and Z. Kuang, 2016: The linear response function of an idealized atmosphere. Part II: Implications for the practical use of the fluctuation–dissipation theorem and the role of operator's nonnormality. *J. Atmos. Sci.*, **73**, 3441–3452, doi:10.1175/JAS-D-16-0099.1.

Hasselmann, K., 1976: Stochastic climate models. Part I. Theory. *Tellus*, **28**, 473–485, doi:10.3402/tellusa.v28i6.11316.

Held, I. M., and M. J. Suarez, 1994: A proposal for the intercomparison of the dynamical cores of atmospheric general circulation models. *Bull. Amer. Meteor. Soc.*, **75**, 1825–1830, doi:10.1175/1520-0477(1994)075<1825:APFTIO>2.0.CO;2.

James, I. N., and J. P. Dodd, 1996: A mechanism for the low-frequency variability of the mid-latitude troposphere. *Quart. J. Roy. Meteor. Soc.*, **122**, 1197–1210, doi:10.1002/qj.49712253309.

Keeley, S. P. E., R. T. Sutton, and L. C. Shaffrey, 2009: Does the North Atlantic Oscillation show unusual persistence on intraseasonal timescales? *Geophys. Res. Lett.*, **36**, L22706, doi:10.1029/2009GL040367.

Kidson, J. W., 1988: Interannual variations in the Southern Hemisphere circulation. *J. Climate*, **1**, 1177–1198, doi:10.1175/1520-0442(1988)001<1177:IVITSH>2.0.CO;2.

Lee, S., S.-W. Son, K. Grise, and S. B. Feldstein, 2007: A mechanism for the poleward propagation of zonal mean flow anomalies. *J. Atmos. Sci.*, **64**, 849–868, doi:10.1175/JAS3861.1.

Leith, C. E., 1975: Climate response and fluctuation dissipation. *J. Atmos. Sci.*, **32**, 2022–2026, doi:10.1175/1520-0469(1975)032<2022: CRAFD>2.0.CO;2.

Lorenz, D. J., and D. L. Hartmann, 2001: Eddy–zonal flow feedback in the Southern Hemisphere. *J. Atmos. Sci.*, **58**, 3312–3327, doi:10.1175/1520-0469(2001)058<3312:EZFFIT>2.0.CO;2.

——, and ——, 2003: Eddy–zonal flow feedback in the Northern Hemisphere winter. *J. Atmos. Sci.*, **16**, 1212–1227, doi:10.1175/1520-0442(2003)16<1212:EFFITN>2.0.CO;2.

Lutsko, N. J., I. M. Held, and P. Zurita-Gotor, 2015: Applying the fluctuation–dissipation theorem to a two-layer model of quasigeostrophic turbulence. *J. Atmos. Sci.*, **72**, 3161–3177, doi:10.1175/JAS-D-14-0356.1.

Majda, A. J., R. Abramov, and M. Grote, 2005: *Information Theory and Stochastics for Multiscale Nonlinear Systems.* American Mathematical Society, 133 pp.

Martynov, R. S., and Yu. M. Nechepurenko, 2004: Finding the response matrix for a discrete linear stochastic dynamical system. *J. Comput. Math. Phys.*, **44**, 771–781, doi:10.1134/S0965542506070062.

North, G. R., R. E. Bell, and J. W. Hardin, 1993: Fluctuation dissipation in a general circulation model. *Climate Dyn.*, **8**, 259–264, doi:10.1007/BF00209665.

Penland, C., 1989: Random forcing and forecasting using principal oscillation pattern analysis. *Mon. Wea. Rev.*, **117**, 2165–2185, doi:10.1175/1520-0493(1989)117<2165:RFAFUP>2.0.CO;2.

Polvani, L. M., and P. J. Kushner, 2002: Tropospheric response to stratospheric perturbations in a relatively simple general circulation model. *Geophys. Res. Lett.*, **29**, doi:10.1029/2001GL014284.

Ring, M. J., and R. A. Plumb, 2007: Forced annular mode patterns in a simple atmospheric general circulation model. *J. Atmos. Sci.*, **64**, 3611–3626, doi:10.1175/JAS4031.1.

——, and ——, 2008: The response of a simplified GCM to axisymmetric forcings: Applicability of the fluctuation–dissipation theorem. *J. Atmos. Sci.*, **65**, 3880–3898, doi:10.1175/2008JAS2773.1.

Robinson, W. A., 1994: Eddy feedbacks on the zonal index and eddy–zonal flow interactions induced by zonal flow transience. *J. Atmos. Sci.*, **51**, 2553–2562, doi:10.1175/1520-0469(1994)051<2553: EFOTZI>2.0.CO;2.

——, 2000: A baroclinic mechanism for the eddy feedback on the zonal index. *J. Atmos. Sci.*, **57**, 415–422, doi:10.1175/1520-0469(2000)057<0415:ABMFTE>2.0.CO;2.

Sheshadri, A., and R. A. Plumb, 2016: Sensitivity of the surface responses of an idealized AGCM to the timing of imposed ozone depletion-like polar stratospheric cooling. *Geophys. Res. Lett.*, **43**, 2330–2336, doi:10.1002/2016GL067964.

——, ——, and D. I. V. Domeisen, 2014: Can the delay in Antarctic polar vortex breakup explain recent trends in surface westerlies? *J. Atmos. Sci.*, **71**, 566–573, doi:10.1175/JAS-D-12-0343.1.

——, ——, and E. P. Gerber, 2015: Seasonal variability of the polar stratospheric vortex in an idealized AGCM. *J. Atmos. Sci.*, **72**, 2248–2266, doi:10.1175/JAS-D-14-0191.1.

Son, S.-W., and S. Lee, 2006: Preferred modes of variability and their relationship with climate change. *J. Climate*, **19**, 2063–2075, doi:10.1175/JCLI3705.1.

Sparrow, S., M. Blackburn, and J. D. Haigh, 2009: Annular variability and eddy–zonal flow interactions in a simplified atmospheric GCM. Part I: Characterization of high- and low-frequency behavior. *J. Atmos. Sci.*, **66**, 3075–3094, doi:10.1175/2009JAS2953.1.

Thompson, D. W. J., and J. M. Wallace, 2000: Annular modes in the extratropical circulation. Part I: Month-to-month variability. *J. Climate*, **13**, 1000–1016, doi:10.1175/1520-0442(2000)013<1000: AMITEC>2.0.CO;2.

——, ——, and G. C. Hegerl, 2000: Annular modes in the extratropical circulation: Part II: Trends. *J. Climate*, **13**, 1018–1036, doi:10.1175/1520-0442(2000)013<1018:AMITEC>2.0.CO;2.

von Storch, H., T. Bruns, I. Fischer-Burns, and K. Hasselmann, 1988: Principal oscillation pattern analysis of the 30- to 60-day oscillation in general circulation model equatorial troposphere. *J. Geophys. Res.*, **93**, 11 022–11 036, doi:10.1029/JD093iD09p11022.

Watterson, I. G., 2002: Wave–mean flow feedback and the persistence of simulated zonal flow vacillation. *J. Atmos. Sci.*, **59**, 1274–1288, doi:10.1175/1520-0469(2002)059<1274: WMFFAT>2.0.CO;2.

——, 2007: Southern "annular modes" simulated by a climate model—Patterns, mechanisms, and uses. *J. Atmos. Sci.*, **64**, 3113–3131, doi:10.1175/JAS4014.1.